

DYNAMICAL SAMPLING WITH ADDITIVE RANDOM NOISE

AKRAM ALDROUBI, LONGXIU HUANG, ILYA KRISHTAL,
AKOS LEDECZI, ROY R. LEDERMAN, PETER VOLGYESI

ABSTRACT. Dynamical sampling deals with signals that evolve in time under the action of a linear operator. The purpose of the present paper is to analyze the performance of the basic dynamical sampling algorithms in the finite dimensional case and study the impact of additive noise. The algorithms are implemented and tested on synthetic and real data sets, and denoising techniques are integrated to mitigate the effect of the noise. We also develop theoretical and numerical results that validate the algorithm for recovering the driving operators, which are defined via a real symmetric convolution.

2010 AMS Mathematics Subject Classification — Primary 94A20, 94A12; Secondary 42C15, 15A29.

1. INTRODUCTION

Dynamical sampling is a framework for processing signals that evolve in time under the action of a linear operator. In dynamical sampling, one seeks to exploit the association between the signals received at various time levels to enhance the classical sampling and reconstruction techniques or propose novel sampling and reconstruction algorithms. Since the original work on dynamical sampling [5], a number of subsequent studies have been devoted to various aspects of the theory and applications (see, for example, [1, 2, 3, 4, 6, 8, 9, 10, 13, 14, 15, 18, 20, 21, 22, 23, 25, 26, 27]).

The present study addresses certain numerical and theoretical aspects of the two main problems of dynamical sampling in the finite dimensional setting. The first problem is to recover a signal f that evolves in time under the action of a known operator A [4, 5]. The second problem is to recover the driving operator A in the case when it is unknown or only partially known [8]. The main contributions of this study are as follows: (a) performance evaluation of basic algorithms developed within the dynamical sampling framework; (b) analysis of the impact of additive noise and the effectiveness of denoising techniques, when

Date: October 16, 2018.

2010 Mathematics Subject Classification. Primary 94A20, 94A12, 42C15, 15A29.

Key words and phrases. Distributed sampling, reconstruction, channel estimation, spectral estimation, systems from iterative actions of an operator, frames from iterations of operators, mobile sampling.

processing real and synthetic data sets. A preliminary version of this study has been documented in [7].

As we mentioned above, the first problem of dynamical sampling is concerned with the recovery of a signal f that evolves in time under the action of a known operator A . More precisely, we consider a signal $f \in \mathbb{C}^d$ and a bounded linear operator A on \mathbb{C}^d which we identify with its matrix in the standard basis. At time level $n \in \mathbb{N}$, the signal becomes

$$(1.1) \quad f_n = A^n f.$$

We let $\Omega \subset \{1, \dots, d\}$ denote a set of ‘‘spatial’’ locations. The noiseless dynamical samples are then

$$(1.2) \quad \{f_n(j) : j \in \Omega, 0 \leq n \leq L\}.$$

In [4], necessary and sufficient conditions for recovering $f \in \mathbb{C}^d$ have been derived in terms of A , Ω , and L .

In the noisy case, we consider the corrupted dynamical samples of the form

$$(1.3) \quad \{f_n(j) + \eta_n(j), j \in \Omega, 0 \leq n \leq L\},$$

where η_n , $n \geq 0$ are independent identically distributed (i.i.d.) d -dimensional random variables with zero mean and covariance matrix $\sigma^2 I$, and $\eta_n(j)$ denotes the j -th component of η_n .

Using the $d \times d$ diagonal sub-sampling matrix S_Ω , defined by

$$(1.4) \quad (S_\Omega)_{jj} = \begin{cases} 1 & j \in \Omega \\ 0 & \text{otherwise,} \end{cases}$$

the noisy data sampled at time level n in (1.3) can be described by the vectors \tilde{y}_n given by

$$(1.5) \quad \tilde{y}_n = S_\Omega(f_n + \eta_n)$$

The signal f can be approximately recovered from the noisy measurements \tilde{y}_n by solving the least squares minimization problem

$$(1.6) \quad f_L^\sharp = \arg \min_g \sum_{n=0}^L \|S_\Omega(A^n g) - \tilde{y}_n\|_2^2.$$

In this study, an iterative algorithm for solving problem (1.6) is investigated. In addition, the mean squared error (MSE) $E(\|\epsilon_L\|^2)$ is estimated with $\epsilon_L = f_L^\sharp - f$ and the behavior of the MSE is analyzed as $L \rightarrow \infty$ for an unbiased linear estimator.

The second problem of dynamical sampling deals with the case when the evolution operator A is unknown (or only partially known). In [8], an algorithm has been proposed for finding the spectrum of A from the dynamical samples. The present paper delves deeper into this algorithm from both theoretical and numerical perspectives. From the theoretical perspective, an alternative proof is given

for the fact that the algorithm in [8] can (almost surely) recover the spectrum of A from dynamical samples and also recover the operator A itself, in the case when it is known that A is given by a circular convolution $Af = a * f$ with some real symmetric filter a in \mathbb{R}^d . From a numerical point of view, this analytical result lays the theoretical foundation and paves the way toward recovering the operator A and the signal from real data collected from physical processes such as the heat diffusion. The nature of the spectrum recovery algorithm also motivates an integration of Cadzow-like denoising techniques [12, 16], which can be applied to both synthetic and real data.

1.1. Contribution and Organization. In Section 2, we summarize the notation that is used throughout the paper and present the algorithms for signal and filter recovery that work ideally in the noiseless case. To recover the signal, we borrow a least squares updating technique from [11] and tailor it for dynamical sampling. To recover the driving operator (in the case of a convolution), we review the algorithm from [8] and provide its new derivation, which is more straightforward than the general proof in [8]. In Section 3, the Cadzow denoising method is sketched for a special case of uniform sub-sampling; it is validated to be numerically efficient in the context of dynamical sampling in Section 5. Section 4 is dedicated to the error analysis of the least squares solutions for finding the original signal in the presence of additive white noise. It shows the relation between the MSE of the solution and the number of time levels considered. In Section 5, we outline the outcomes of the extensive tests performed for the algorithms discussed in Sections 2 and 3. More precisely, Section 5.1 demonstrates the consistency of the theory for the MSE of the least squares solutions on synthetic data. Section 5.2 illustrates the effect of Cadzow denoising method on signal and filter recovery in the case of synthetic data. Finally, in Section 5.3, the recovery algorithms and denoising techniques are integrated together to process real data collected from cooling processes.

2. NOTATION AND PRELIMINARIES

2.1. Notation. Let \mathbb{Z} be the set of all integers and \mathbb{Z}_d be the cyclic group of order d . By \mathbb{C}^d and $\mathbb{C}^{m \times d}$ we denote the linear space of all column vectors with d complex components and the space of complex matrices of dimension $m \times d$, respectively. Given a matrix $A \in \mathbb{C}^{m \times d}$, A_{ij} stands for the entry of the i -th row and j -th column of A , A^* represents the conjugate transpose of A , and the 2-norm of A is defined by

$$\|A\| = \sup_{f \in \mathbb{C}^d, \|f\|_2=1} \|Af\|_2,$$

where $\|f\|_2 = \sqrt{\sum_{i=1}^d |f(i)|^2}$ and $f(i)$ refers to i -th component of a vector $f \in \mathbb{C}^d$.

For a random variable x that is distributed normally with mean μ and variance σ^2 , we may write $x \sim N(\mu, \sigma^2)$.

2.2. A general least squares updating technique for signal recovery. We borrow from [17] the following updating technique for adjusting a least squares solution when new equations are added. Consider the following least squares problem

$$(2.1) \quad f_L^\# = \arg \min_{g \in \mathbb{C}^d} \sum_{i=1}^L \|A_i g - b_i\|_2^2,$$

where $A_i \in \mathbb{C}^{m_i \times d}$, and $\text{rank}(A_1) = d$ (i.e., A_1 has full column rank).

We take the case of $L = 2$ as an example to explain the updating technique. Consider the QR decomposition $A_1 = Q_1 R_1$, where Q_1 is an $m_1 \times d$ matrix satisfying $Q_1^* Q_1 = I$ and R_1 is a $d \times d$ triangular matrix. Then

$$f_1^\# = \arg \min_g \|A_1 g - b_1\|_2^2 = \arg \min_g \|R_1 g - Q_1^* b_1\|_2^2.$$

Let $\tilde{b}_1 = Q_1^* b_1$. Since A_1 has full rank, we have $f_1^\# = R_1^{-1} \tilde{b}_1$. Suppose that new information is added, then the least squares problem and its solution needs to be updated, i.e., $f_2^\# = \arg \min_{g \in \mathbb{C}^d} \sum_{i=1}^2 \|A_i g - b_i\|_2^2$.

To solve the new least squares problem, we note that

$$\begin{aligned} \arg \min_{g \in \mathbb{C}^d} \sum_{i=1}^2 \|A_i g - b_i\|_2^2 &= \arg \min_{g \in \mathbb{C}^d} \left\| \begin{pmatrix} A_1 \\ A_2 \end{pmatrix} g - \begin{pmatrix} b_1 \\ b_2 \end{pmatrix} \right\|_2^2 \\ &= \arg \min_{g \in \mathbb{C}^d} \left\| \begin{pmatrix} Q_1 & 0 \\ 0 & I \end{pmatrix} \begin{pmatrix} R_1 \\ A_2 \end{pmatrix} g - \begin{pmatrix} b_1 \\ b_2 \end{pmatrix} \right\|_2^2 \\ &= \arg \min_{g \in \mathbb{C}^d} \left\| \begin{pmatrix} R_1 \\ A_2 \end{pmatrix} g - \begin{pmatrix} Q_1^* b_1 \\ b_2 \end{pmatrix} \right\|_2^2 \\ &= \arg \min_{g \in \mathbb{C}^d} \left\| \begin{pmatrix} R_1 \\ A_2 \end{pmatrix} g - \begin{pmatrix} \tilde{b}_1 \\ b_2 \end{pmatrix} \right\|_2^2. \end{aligned}$$

Therefore, the problem reduces to finding

$$f_2^\# = \arg \min_{g \in \mathbb{C}^d} \left\| \begin{pmatrix} R_1 \\ A_2 \end{pmatrix} g - \begin{pmatrix} \tilde{b}_1 \\ b_2 \end{pmatrix} \right\|_2^2.$$

One further needs to calculate the QR decomposition

$$\begin{pmatrix} R_1 \\ A_2 \end{pmatrix} = Q_2 R_2,$$

where Q_2 is a unitary matrix and R_2 is a $d \times d$ triangular matrix. Denote

$$\tilde{b}_2 = Q_2^* \begin{pmatrix} \tilde{b}_1 \\ b_2 \end{pmatrix}.$$

It follows that $f_2^\# = R_2^{-1} \tilde{b}_2$.

The same process can be applied to the case $L \geq 3$ which leads to the iterated updating algorithm that is summarized in Algorithm 1.

This algorithm demonstrates that the recovery problem in dynamical sampling can be solved in a streaming setup, where the solution is updated as new measurements are collected over time,

1. without storing all the previous samples (b_j) or explicitly rewriting all the matrices (A_j) for all $j < i$ at the i th step,
2. and taking advantage of quantities that are stored from previous iterations to avoid the naive computation involving all the previous samples and matrices.

Observe that in the dynamical sampling framework we have $A_i = S_\Omega A^{i-1}$. Assume that at step i , the QR decomposition for

$$\mathcal{A}_i = \begin{pmatrix} S_\Omega I \\ S_\Omega A \\ \vdots \\ S_\Omega A^{i-1} \end{pmatrix}$$

is

$$\mathcal{A}_i = QR.$$

At step $i + 1$, \mathcal{A}_{i+1} can thus be written in the convenient form

$$\begin{pmatrix} S_\Omega I \\ QRA \end{pmatrix} = \begin{pmatrix} I & 0 \\ 0 & Q \end{pmatrix} \begin{pmatrix} S_\Omega I \\ RA \end{pmatrix}.$$

Goal: Recover the original signal by processing time series data.

Input A_1, b_1

Set $A_1 = Q_1 R_1$, the economic QR decomposition of A_1 with the assumption that A_1 has full column rank (see Remark 4.1).

Set $\tilde{b}_1 = Q_1^* b_1$.

Set $f_1^\sharp = R_1^{-1} \tilde{b}_1$.

for $i = 2$ **to** L **do**

Input A_i, b_i

Compute the QR decomposition for $\begin{pmatrix} R_{i-1} \\ A_i \end{pmatrix} = Q_i R_i$ using the Householder transformation [17].

Set $\tilde{b}_i = Q_i^* \begin{pmatrix} \tilde{b}_{i-1} \\ b_i \end{pmatrix}$.

Set $f_i^\sharp = R_i^{-1} \tilde{b}_i$.

end

Output f_L^\sharp

Algorithm 1: Pseudo-code of the iterated updating algorithm.

2.3. Filter recovery for the special case of convolution operators and uniform subsampling. In this section, we recall from [8] an algorithm for recovering an unknown driving operator A that is defined via a convolution with a real symmetric filter i.e., A is a circulant matrix corresponding to a convolution with a : $Af = a * f$, and where the spatial sampling is uniform at every time-instant n . We also provide a new, direct proof of validity for the filter recovery algorithm for this case. Specifically, we consider samples of $A^\ell f = a^\ell * f$ at $m\mathbb{Z}_d$ where $m \geq 2$, and $a^\ell = a * \dots * a$ is the ℓ times convolution of the filter a . We also assume that the Fourier transform \hat{a} of the filter a is real symmetric, and strictly decreasing on $[0, \frac{d-1}{2}]$. We will use the notation $S_m f_n$ to describe this uniform subsampling. In particular, for a vector $z \in \ell^2(\mathbb{Z}_d)$, $S_m z$ belongs to $\ell^2(\mathbb{Z}_J)$, and $S_m z(j) = z(mj)$ for $j = 1, \dots, J$, where throughout we will assume that m is odd, and $d = Jm$ for some odd integer J .

Let

$$(2.2) \quad y_\ell = S_m(A^\ell f) = S_m(a^\ell * f), \quad \ell \geq 0,$$

be the dynamical samples at time level ℓ . By Poisson's summation formula,

$$(2.3) \quad (\widehat{S_m z})(j) = \frac{1}{m} \sum_{n=0}^{m-1} \hat{z}(j + nJ), \quad 0 \leq j \leq J-1, \quad z \in \ell^2(\mathbb{Z}_d),$$

An application of the Fourier transform to (2.2) yields

$$(2.4) \quad \hat{y}_\ell(j) = \frac{1}{m} \sum_{n=0}^{m-1} \hat{a}^\ell(j + nJ) \hat{f}(j + nJ), \quad 0 \leq j \leq J-1.$$

For each fixed $j \in \mathbb{Z}_J$ and for some integer L with $L \geq 2m-1$ ($L = 2m-1$ is the minimum number of time levels that we need to recover the filter), we introduce the following notation:

$$\begin{aligned} \bar{y}_\ell(j) &= (\hat{y}_\ell(j), \hat{y}_{\ell+1}(j), \dots, \hat{y}_{\ell+L}(j))^T, \\ \bar{f}(j) &= (\hat{f}(j), \hat{f}(j+J), \dots, \hat{f}(j+(m-1)J))^T, \end{aligned}$$

and

$$(2.5) \quad \mathcal{V}_m(j) = \begin{pmatrix} 1 & 1 & \dots & 1 \\ \hat{a}(j) & \hat{a}(j+J) & \dots & \hat{a}(j+(m-1)J) \\ \vdots & \vdots & \vdots & \vdots \\ \hat{a}^{L-1}(j) & \hat{a}^{L-1}(j+J) & \dots & \hat{a}^{L-1}(j+(m-1)J) \end{pmatrix},$$

where $0 \leq j \leq J-1$. From (2.4), it follows that

$$(2.6) \quad \bar{y}_\ell(j) = \frac{1}{m} \mathcal{V}_m(j) D^\ell(j) \bar{f}(j), \quad \text{for } 0 \leq j \leq J-1, \quad \ell \geq 0,$$

where $D(j)$ is the diagonal matrix $D(j) = \text{diag}(\hat{a}(j), \hat{a}(j+J), \dots, \hat{a}(j+(m-1)J))$. Let $p_j(x) = c_0(j) + c_1(j)x + \dots + c_{m-1}(j)x^{m-1} + x^m$ be the minimal polynomial that annihilates $D(j)$. The degree of p_j is equal to the number of distinct diagonal

values of $D(j)$. Since $L \geq 2m - 1$, it follows from the assumptions on \hat{a} (\hat{a} is real symmetric, and strictly decreasing on $[0, \frac{d-1}{2}]$) that $\deg(p_j) = m$ for $j \neq 0$ and $\deg(p_0) = (m + 1)/2$. Moreover, the rectangular Vandermonde matrix $\mathcal{V}_m(j)$ has rank $r_j = m$ if $j \neq 0$, and $r_0 = (m + 1)/2$ if $j = 0$. Consequently, using (2.6), we have that for almost all \hat{f} ,

$$(2.7) \quad \bar{y}_{k+r_j}(j) + \sum_{\ell=0}^{r_j-1} c_\ell(j) \bar{y}_{k+\ell}(j) = 0, \quad 0 \leq j \leq J - 1,$$

where $c_\ell(j)$ are the coefficients of the polynomial p_j and $r_j = \deg p_j = \text{rank } \mathcal{V}_m(j)$. The above discussion leads to the following Algorithm 2 for recovering the spectrum $\sigma(A)$.

Goal: Recover the spectrum $\sigma(A)$.

Set $J = d/m$.

for $j = 0$ **to** $J - 1$ **do**

Find the minimal integer r_j for which the system (2.7) has a solution $c(j)$ and find the solution;

set $p_j(\lambda) = \lambda^{r_j} + \sum_{\ell=0}^{r_j-1} c_\ell(j) \lambda^\ell$ and find the set $R(j)$ of all roots of p_j .

end

Set $\sigma(A) = \bigcup_{j=0}^{J-1} R(j)$.

Algorithm 2: A spectrum recovery algorithm for convolution operators.

Remark 2.1. *The algorithm for spectrum recovery involves finding the roots of a set polynomials of degree m or $\frac{m+1}{2}$, where m is the subsampling factor. This problem becomes more and more difficult as m becomes larger and larger. However, in applications, one could expect m to be of moderate size ($m \leq 5$). Moreover, if some of the spectral values are too close to each other, then finding the coefficients of the minimal polynomials becomes unstable.*

Remark 2.2. *The recovery of both the filter and the signal from the measurements points to certain relations to the problem of Blind Deconvolution (see for example [19]); typically, Blind Deconvolution does not involve the difficulty arising from the sub-sampling (the operator S_m), but it is restricted to one time measurement, and uses other assumptions on the signal and filter.*

3. CADZOW DENOISING METHOD

In this section, we describe a Cadzow-like algorithm (see Algorithm 3) [12, 16] which can be effectively applied to approximate the dynamical samples y_n in (2.2) from the noisy measurements $\tilde{y}_n = y_n + \eta_n$.

Suppose data points y_n in (2.2) are such that m is an odd integer and A is a symmetric circulant matrix generated by a real symmetric filter a , i.e., the

Fourier transform \hat{a} of the filter a is real symmetric. In addition, we also assume that \hat{a} is monotonic on $[0, \frac{d-1}{2}]$. Let L be the number of time levels as in (2.5). In particular, it is necessary that $L \geq 2m - 1$. Without loss of generality we assume that L is even. From (2.4), (2.6), (2.7) in Section 2.3 (see also [5, 8]), it follows that the Hankel matrix

$$(3.1) \quad H(j) = \begin{pmatrix} \hat{y}_0(j) & \hat{y}_1(j) & \cdots & \hat{y}_{\frac{L}{2}}(j) \\ \hat{y}_1(j) & \hat{y}_2(j) & \cdots & \hat{y}_{\frac{L}{2}+1}(j) \\ \vdots & \vdots & \vdots & \vdots \\ \hat{y}_{\frac{L}{2}}(j) & \hat{y}_{\frac{L}{2}+1}(j) & \cdots & \hat{y}_L(j) \end{pmatrix},$$

has rank m for $j \neq 0$ and $(m+1)/2$ for $j = 0$. However, the matrices $\tilde{H}(j)$ formed as in (3.1) using the noisy measurements \tilde{y}_n will fail the rank conditions. Cadzow's Algorithm approximates $H(j)$ via iterative changes of $\tilde{H}(j)$ that enforce the rank and the Hankel conditions successively.

Goal : Denoising measurements matrix $\tilde{Y} = (\tilde{y}_0 \ \tilde{y}_1 \ \dots \ \tilde{y}_L)$.
Input : \tilde{Y} and k_{\max} (maximal number of iterations).

Generate the matrix $(\tilde{Y})^\wedge$ by taking the Fourier transform on \tilde{Y} .

for $j = 0$ **to** $J - 1$ **do**

if $j = 0$, **then**

Set $r = \frac{m+1}{2}$

end

else Set $r = m$;

Form Hankel matrix $X = \tilde{H}(j)$ as in (3.1) from the j th row of $(\tilde{Y})^\wedge$.

for $k = 1$ **to** k_{\max} **do**

Compute the SVD of X : $X = U\Sigma V^*$,
 $\Sigma = \text{diag}(\sigma_1, \dots, \sigma_{\frac{L}{2}+1})$.
Set $X = U \text{diag}(\sigma_1, \dots, \sigma_r, 0, \dots, 0) V^*$.
Generate a Hankel matrix H_{new} by averaging X across its anti-diagonals.
Set $X = H_{\text{new}}$.

end

Update the j th row of $(\tilde{Y})^\wedge$ by the vector obtained by averaging the anti-diagonals of X .

end

Update \tilde{Y} by taking inverse Fourier transform on $(\tilde{Y})^\wedge$.

Output: Denoised data \tilde{Y} .

Algorithm 3: The pseudo-code for the Cadzow denoising method.

For each $j \in \mathbb{Z}_J$, an application of the singular value decomposition (SVD) technique produces a decomposition $\tilde{H}(j) = U\Sigma V^*$, where $\Sigma = \text{diag}(\sigma_1, \dots, \sigma_{\frac{L}{2}+1})$ and $\sigma_1 \geq \dots \geq \sigma_{\frac{L}{2}+1}$. Since the rank is known to be r_j , one can set $\sigma_i = 0$ for $i > r_j$ and obtain an amended matrix of singular values Σ_{r_j} . Then, one may proceed to compute the matrix $X_{new} = U\Sigma_{r_j}V^*$ and form a new Hankel matrix H_{new} by averaging X_{new} across its anti-diagonals. This procedure is applied iteratively. After several iterations, a better approximation of the Hankel matrix $H(j)$ is obtained and a vector of denoised data can be retrieved by applying the inverse Fourier transform.

4. ERROR ANALYSIS

4.1. Error analysis for general least squares problems. We begin this section with the error analysis of a least squares problem that is more general than the first dynamical sampling problem. We let $A_i \in \mathbb{C}^{m_i \times d}$, $f \in \mathbb{C}^d$, and $\tilde{y}_i = A_i f + \eta_i$, where η_i are i.i.d. random variables with a zero mean and a variance matrix $\sigma^2 I$. The signal f can be approximately recovered via

$$(4.1) \quad f_L^\# = \arg \min_g \sum_{i=1}^L \|A_i g - \tilde{y}_i\|_2^2.$$

Denote the error $\epsilon_L = f_L^\# - f$. By (4.1) and the definition for \tilde{y}_i , it follows that

$$(4.2) \quad \epsilon_L = \arg \min_\epsilon \sum_{i=1}^L \|A_i \epsilon - \eta_i\|_2^2.$$

Let

$$(4.3) \quad \mathcal{A}_L = \begin{pmatrix} A_1 \\ A_2 \\ \vdots \\ A_L \end{pmatrix},$$

and assume that for $L \geq N$, where N is some fixed number, \mathcal{A}_L , defined by (4.3) above, has full rank. By solving problem (4.2), we have

$$(4.4) \quad \epsilon_L = \left(\sum_{i=1}^L A_i^* A_i \right)^{-1} \sum_{i=1}^L A_i^* \eta_i, \text{ for all } L \geq N.$$

The following proposition can be derived from [24, Theorem B on p. 574]. For the convenience of the reader, however, we include the proof in the Appendix.

Proposition 4.1. *Assume that \mathcal{A}_L is defined as in (4.3) and has full rank for $L \geq N$. Let $\lambda_j(L)$, $1 \leq j \leq d$, denote the eigenvalues of the matrix $\mathcal{A}_L^* \mathcal{A}_L =$*

$\sum_{i=1}^L A_i^* A_i$, $1 \leq j \leq d$. Then, the following holds:

$$(4.5) \quad E(\|\epsilon_L\|_2^2) = \sigma^2 \sum_{j=1}^d 1/\lambda_j(L),$$

where ϵ_L is obtained from (4.2) and σ is the variance of the noise.

To study the behavior of the MSE function in (4.5), we recall the well-known Courant-Fischer Minimax Theorem and one of its most useful corollaries.

Theorem 4.2. (Courant-Fischer Minimax Theorem) *Let A be a $d \times d$ Hermitian matrix with eigenvalues $\lambda_1 \geq \dots \geq \lambda_k \geq \dots \geq \lambda_d$. Then,*

$$\lambda_k = \max_U \left\{ \min_x \left\{ \frac{x^* A x}{x^* x} : x \in U \text{ and } x \neq 0 \right\} : \dim(U) = k \right\}.$$

Corollary 4.3. *Let $A \in \mathbb{C}^{d \times d}$ and $B \in \mathbb{C}^{d \times d}$ be self-adjoint positive semidefinite matrices. Then, $\lambda_i(A + B) \geq \lambda_i(A)$ and $\lambda_i(A + B) \geq \lambda_i(B)$.*

The following result is immediate from Corollary 4.3.

Proposition 4.4. *The function $E(\|\epsilon_L\|_2^2)$ defined by (4.5) is a non-negative non-increasing function of L for $L \geq N$ where N is some fixed number, such that \mathcal{A}_N in (4.3) has full rank. Consequently, as L goes to ∞ , it converges to a non-negative constant.*

The goal of the following example is to illustrate the above result in the context of dynamical sampling but without sub-sampling.

Example 4.1 (Special case: no sub-sampling). *Suppose that A is a normal matrix and suppose that $A_i = A^{i-1}$ in (4.2). Because A is normal, it can be written as $A = U^* D U$, where U is a unitary matrix and D is a diagonal matrix with the diagonal entries s_1, s_2, \dots, s_d . Hence, $\mathcal{A}_L^* \mathcal{A}_L$ can be computed as*

$$(4.6) \quad \mathcal{A}_L^* \mathcal{A}_L = \sum_{k=1}^L (A^*)^{k-1} A^{k-1} = U^* \sum_{k=1}^L (D^* D)^{k-1} U.$$

Defining $\Lambda = \Lambda(L)$ by

$$\mathcal{A}_L^* \mathcal{A}_L = U^* \Lambda U,$$

and

$$\Lambda = \begin{pmatrix} \lambda_1(L) & & \\ & \ddots & \\ & & \lambda_d(L) \end{pmatrix},$$

we get from (4.6) that

$$\lambda_j(L) = \begin{cases} \frac{1-|s_j|^{2L}}{1-|s_j|^2}, & |s_j| \neq 1; \\ L, & |s_j| = 1. \end{cases}$$

The error ϵ_L can be represented as

$$\epsilon_L = \left(\sum_{i=1}^L A_i^* A_i \right)^{-1} \sum_{i=1}^L A_i^* \eta_i = U^* \Lambda^{-1} \sum_{i=1}^L (D^*)^{i-1} U \eta_i,$$

and (4.5) follows immediately for this special case.

To illustrate Proposition 4.4, note that, when $|s_j| < 1$, the expression $\frac{1}{\lambda_j(L)} = \frac{1-|s_j|^2}{1-|s_j|^{2L}}$ decreases and converges to $1 - |s_j|^2$ as n increases and tends to ∞ .

When $|s_j| = 1$, then $\frac{1}{\lambda_j(L)} = \frac{1}{L}$ which decreases as L increases.

When $|s_j| > 1$, $\frac{1}{\lambda_j(L)} = \frac{1-|s_j|^2}{1-|s_j|^{2L}}$ decreases (as L increases) and converges to 0 as $L \rightarrow \infty$.

Thus, in all three cases the function $E(\|\epsilon_L\|_2^2)$ is decreasing as L increases. In addition,

$$E(\|\epsilon_L\|_2^2) \rightarrow \sigma^2 \sum_{\substack{1 \leq j \leq d \\ |s_j| < 1}} (1 - |s_j|^2), \text{ as } L \rightarrow \infty.$$

4.2. Error analysis for dynamical sampling. To derive a similar result for dynamical sampling, we replace the general operator A_i in (4.2) with the $i - 1$ power A^{i-1} of a matrix A followed by a subsampling matrix S_Ω , i.e., we let $A_i = S_\Omega(A^{i-1})$. By Propositions 4.1 and 4.4, and using the fact that $S_\Omega^* S_\Omega = S_\Omega$, the following assertions hold.

Theorem 4.5. *Let $\lambda_j(L)$ denote the j -th eigenvalue of the matrix $\sum_{i=0}^{L-1} (A^*)^i S_\Omega A^i$. Then*

$$E(\|\epsilon_L\|_2^2) = \sigma^2 \sum_{j=1}^d 1/\lambda_j(L),$$

is non-increasing as a function of L . Hence, it converges to some constant as $L \rightarrow \infty$.

Remark 4.1. *The theorem above shows how the mean squared error depends on Ω , A and L . However, for a given A , not all choices of Ω are allowable: there are necessary and sufficient conditions on the choice of Ω that will allow us to reconstruct f by solving (4.1) when $A_i = S_\Omega(A^{i-1})$ and no noise is present [4] (i.e., A_1 is full rank and $\lambda_j(L) > 0$ for all j, L).*

5. NUMERICAL RESULTS

5.1. Error Analysis. In this section, we illustrate the performance of the least squares based method for signal recovery (i.e., Algorithm 1) in the case when the dynamical samples are corrupted by noise. We describe the numerical simulations that we conducted using synthetic data and examine the behavior of $E(\|\epsilon_L\|_2^2/\sigma^2)$ as a function of the number of time levels L .

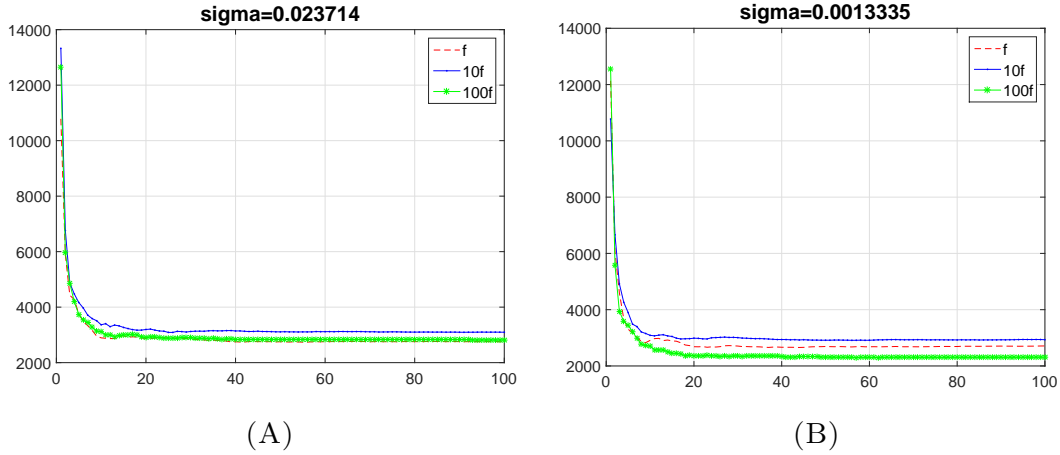


FIGURE 1. The behavior of $E(\|\epsilon_L\|_2^2/\sigma^2)$ for different signals. Here, the curves in (1A) and (1B) show the results with noise variances 2.3714×10^{-2} and 1.3335×10^{-3} , respectively. The signal f is randomly generated with norm 2.2914. Three signals f , $10f$, and $100f$ are used for the simulations, where x -axis stands for the time levels and y -axis represents the value of $E(\|\epsilon_L\|_2^2/\sigma^2)$.

To obtain synthetic data for the simulation, we use a random signal $f \in \ell^2(\mathbb{Z}_{18})$ and a convolution operator $Af = a * f$, determined by a real symmetric vector a with non-zero components given by $(\frac{1}{8}, \frac{1}{2}, 1, \frac{1}{2}, \frac{1}{8})$, i.e., $A \in \mathbb{R}^{18 \times 18}$ is a circulant matrix with the first row $(1, 1/2, 1/8, 0, \dots, 0, 1/8, 1/2)$. We generate the signals $f_i = A^i f$ at time levels $i = 0, 1, \dots, L$. The non-uniform locations $\Omega = \{1, 5, 7, 10, 13, 15, 18\}$ are chosen to generate the samples $\{f_i(j) : j \in \Omega\}$. Independent and identically distributed Gaussian noise with zero mean is then added to the samples to obtain a set of noisy data $\{f_i(j) + \eta_i(j) : j \in \Omega\}$.

Figure 1 shows the relationship between $E(\|\epsilon_L\|_2^2/\sigma^2)$ and the time levels, where ϵ_L is defined by (4.2). For each L , the simulation was repeated 100 times with the same distribution of noise, and $E(\|\epsilon_L\|_2^2/\sigma^2)$ was estimated by averaging the 100 values of $\|\epsilon_L\|_2^2/\sigma^2$. Figure 1A shows how $E(\|\epsilon_L\|_2^2/\sigma^2)$ changes as L varies for three different signals: f , $10f$, and $100f$, where the noise variance is $\sigma = 2.3714 \times 10^{-2}$ and the 2-norm of f approximately equals 2.2914. The graph of $10f$ is given in Figure 2A. Figure 1B shows the behavior of $E(\|\epsilon_L\|_2^2/\sigma^2)$ for the same signals as in Figure 2A, where the noise variance is $\sigma = 1.3335 \times 10^{-3}$. As shown in Figure 1, $E(\|\epsilon_L\|_2^2/\sigma^2)$ decreases as n increases and approaches the constant predicted by Theorem 4.5.

Figure 2 depicts the graphs of the reconstructed signals and the original signals $10f$, $100f$, $10g$, and $100g$ in Figures 2A, 2C, 2B, and 2D, respectively, where $f, g \in \mathbb{R}^{18}$ are randomly generated and scaled to the norm 2.2914. The reconstructed signals from the noisy data and the original signals are shown in Figure 2A for $10f$, in Figure 2B for $10g$, in Figure 2C for $100f$, and in Figure 2D for

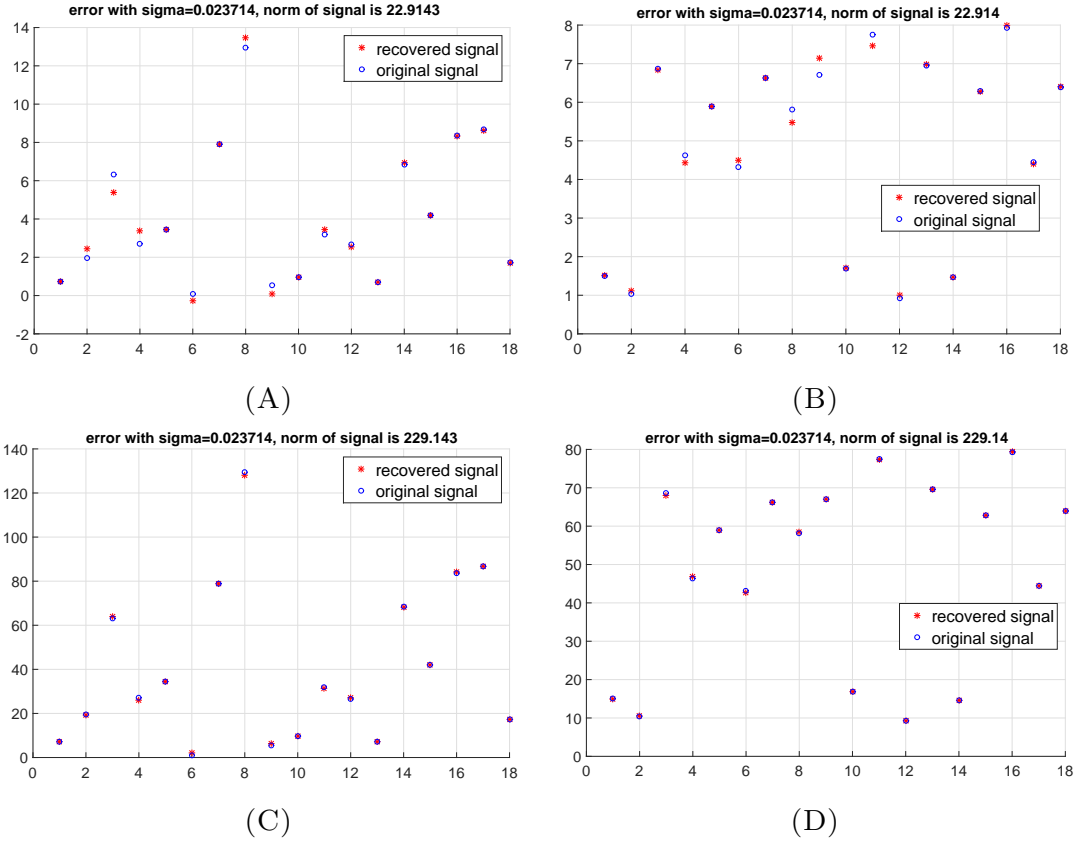


FIGURE 2. The original signals and the reconstructed signals are represented by blue circles and red stars, respectively. The signals in 2C and 2D are obtained from the signals in 2A and 2B, respectively, by multiplying by 10. The norm of the original signal in 2A equals the norm of the original signal in 2B, the same is true for the signals in 2C and 2D.

100g, respectively. The noisy data are corrupted by Gaussian noise with zero mean and standard deviation 2.3714×10^{-2} . As displayed in Figure 2, while the reconstructed signals in Figures 2A and 2B are clearly different from the original signals, it is hard to distinguish the reconstructed signals from the original signals in Figures 2C and 2D because the reconstructed signals are very close to the original signals.

Figures 3 and 4 are simulation results for the sparsely supported signals. For these special signals, a threshold method [24] is introduced for the samples and reconstructed signals. The method is implemented as follows. Let the threshold T be 2σ , let \tilde{y} denote the sample vector, and let f_L^\sharp be the reconstructed signal. If $|\tilde{y}(i)| \leq T$, we set $\tilde{y}(i) = 0$, where $\tilde{y}(i)$ is the i -th component of \tilde{y} . Similarly, if $|f_L^\sharp(i)| \leq T$, we set $f_L^\sharp(i) = 0$. Then the reconstruction results before and

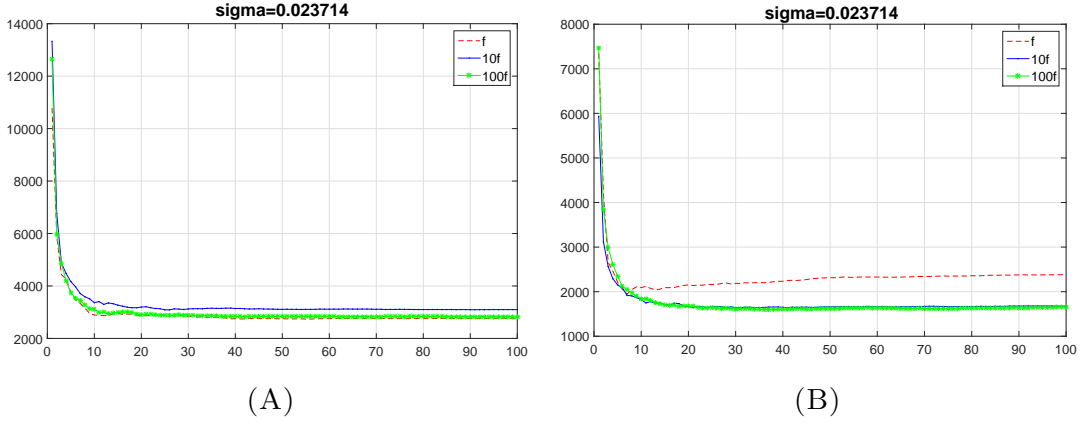


FIGURE 3. The behavior of $E(\|\epsilon_L\|_2^2/\sigma^2)$ are shown in (3A) and (3B) for the sparsely supported signals without and with applying the threshold method, respectively, where the samples are corrupted by Gaussian noise with zero mean and standard deviation 2.3714×10^{-2} .

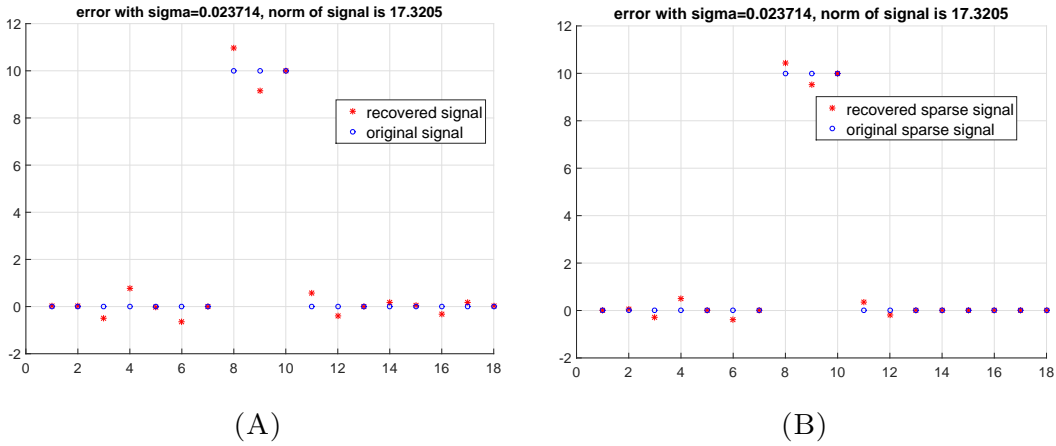


FIGURE 4. A comparison of the reconstruction results before and after applying the threshold method. (4A) and (4B) show the reconstruction results before and after applying the threshold method, respectively. In (4A) and (4B), the original signals have the same sparse support $\{8, 9, 10\}$. The samples are corrupted by the independent Gaussian noise with mean 0 and standard deviation 2.3714×10^{-2} .

after applying the threshold method are compared. Figures 3 and 4 illustrate the behavior of $E(\|\epsilon_L\|_2^2/\sigma^2)$ and the reconstructed signals before and after applying the threshold method, respectively. In the simulation, the samples are corrupted by Gaussian noise with zero mean and standard deviation 2.3714×10^{-2} . A sparsely supported signal $f \in \mathbb{R}^{18}$ is generated with support in the locations $\{8, 9, 10\}$ with $f(8) = f(9) = f(10) = 1$. The MSE $E(\|\epsilon_L\|_2^2/\sigma^2)$ are estimated

for signals f , $10f$, and $100f$ separately. As shown in Figure 3, for n sufficiently large, $E(\|\epsilon_L\|_2^2/\sigma^2)$ is about 20% smaller after the threshold method is applied to the samples and reconstructed signals. Figure 4 shows the graphs of the original signal $10f$ and the reconstructed signal, which suggests that the signal reconstructed by applying the threshold method is more accurate than the one reconstructed without applying the threshold method in the locations outside the support of the original signal. These observations suggest that the threshold method can reduce $E(\|\epsilon_L\|_2^2/\sigma^2)$ by improving the accuracy of the zero sets.

5.2. Cadzow Denoising. In this section, we describe the impact of the Cadzow denoising technique described in Section 3 on dynamical sampling using synthetic data.

5.2.1. Denoising of the sampled data. We use a symmetric convolution operator A with eigenvalues $\{1/8, 1/4, 3/8, 1/2, 5/8, 3/4, 7/8, 1\}$. We let A act on the normalized randomly generated signal $f = (0.2931, 0.3258, 0.04568, 0.3286, 0.2275, 0.0351, 0.1002, 0.1967, 0.3444, 0.34710, 0.0567, 0.3492, 0.3443, 0.1746, 0.2879)^T$ iteratively for 100 times. The iterated signals are stored in a matrix Π as

$$\Pi = (f \ Af \ A^2f \ \dots \ A^{100}f) = (f_0 \ f_1 \ f_2 \ \dots \ f_{100})$$

where $A^k f$ is a column vector for each $0 \leq k \leq 100$ (see (1.1)). At each time level, the generated signals are perturbed by i.i.d. Gaussian noise with zero mean and standard deviation $\sigma \in \{10^{-2}, 10^{-3}, 10^{-4}, 10^{-5}\}$; the noisy signals are denoted by

$$\tilde{\Pi} = \Pi + H,$$

where $H_{i,j} \sim N(0, \sigma^2)$ and every two entries of H are independent (see (1.3)).

The samples are taken uniformly on $3\mathbb{Z}_{15}$ (i.e., $m = 3$), specifically at locations $\Omega = \{1, 4, 7, 10, 13\}$. The Cadzow algorithm (Algorithm 3) is applied to the data $\tilde{Y} = S_m \tilde{\Pi}$ where S_m is defined in the first paragraph of Section 2.3. The denoised data are denoted by Z which is compared to $S_m \Pi$ directly by computing

$$(5.1) \quad \frac{\|Z - S_m \Pi\|}{\|S_m \Pi\|}.$$

In addition, the relative difference between the noisy data $S_m \tilde{\Pi}$ and $S_m \Pi$ is computed as

$$(5.2) \quad \frac{\|S_m \tilde{\Pi} - S_m \Pi\|}{\|S_m \Pi\|}.$$

The same process is repeated for 80 times (with the same Π and different H). The numerical results are obtained by averaging the 80 values of (5.1) and (5.2), respectively.

The simulation results are shown in Figure 5. For $rank \geq 3$, the horizontal values depict the threshold ranks in the Cadzow algorithm. The corresponding vertical values are \log_{10} of the values of (5.1) averaged over 80 repetitions. When

$rank = 0$, (5.2) is used instead of (5.1). As shown in Figure 5, the Cadzow denoising technique works best for noise reduction when the rank of the Hankel matrix is chosen to be 3, which is consistent with the theory described in Section 3.

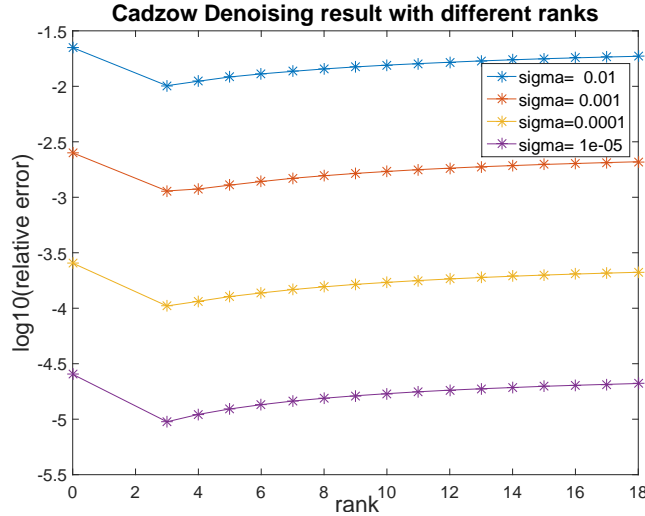


FIGURE 5. The relative errors using Cadzow denoising method. The vertical axis represents \log_{10} of averaged (5.1) when the threshold rank in the Cadzow denoising Algorithm 3 is greater than or equal to 3. When the threshold rank is 0 (5.2) is used instead of (5.1).

In Figure 6, the curve labeled “rank = 0” shows the relationship between \log_{10} of the averaged (5.2) and \log_{10} of the noise standard deviations, while the curves labeled as “rank = r ” for $r = 3, 7, 11, 15$ show the relationship between \log_{10} of the averaged (5.1) and \log_{10} of the noise standard deviation. As displayed in Figure 6, the curves are almost linear. For fixed noise standard deviation, the figure shows that, as predicted by the theory described in Section 3, the best denoising happens when “rank = 3” since the sub-sampling is 3.

5.2.2. *Spectrum Reconstruction of the Convolution Operator.* In order to evaluate the impact of the Cadzow denoising technique when reconstructing the spectrum of the convolution operator, we conducted a number of simulations on synthetic data. We repeated the same process as in Section 5.2.1 until the denoised data Z was generated. Then we used the results of Section 2.3 and Algorithm 2 to recover the spectrum of the convolution operator using separately denoised data Z and noisy data $\tilde{Y} = S_m \tilde{\Pi}$. The simulation results are shown in Figures 7, 8, and 9 for different noise standard deviations. Figure 7 shows the simulation results when the standard deviation of the noise is 10^{-5} . The curves in Figure 7 are simulation results for three different random choices of noise. For Figures 8 and 9, the noise has standard deviations 10^{-4} and 10^{-3} , respectively. As shown

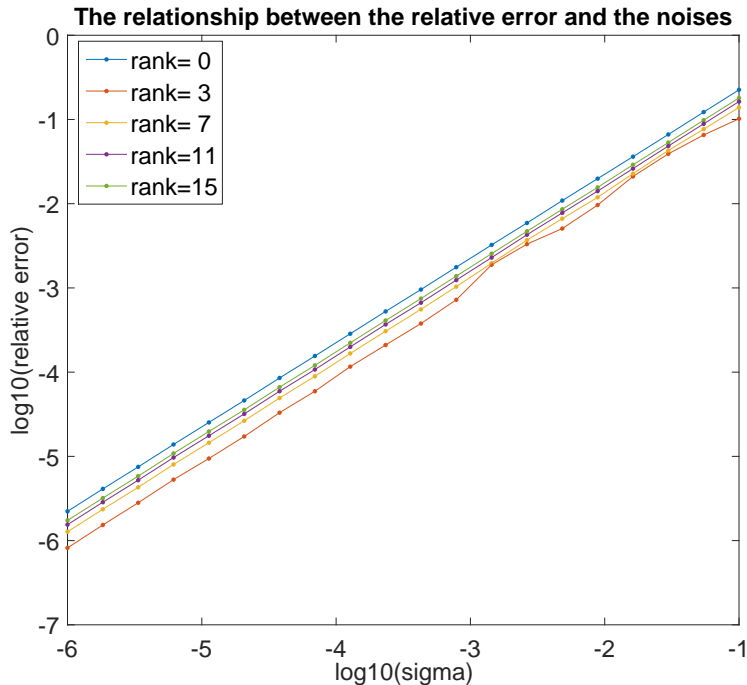


FIGURE 6. The relation between the relative errors and the noise standard deviations using the Cadzow denoising method with different threshold ranks. The curves labeled “rank = r ”, $r = 3, 7 \dots$ reflect the relationship between \log_{10} of the averaged relative errors and \log_{10} of the noise standard deviations, where the relative errors are represented in (5.1) for $\text{rank} \geq 3$ and in (5.2) for $\text{rank} = 0$.

in Figures 7, 8, and 9, the Cadzow denoising technique can make a big difference for the spectrum recovery.

Using the estimated convolution operator and the denoised data, we also evaluated the effectiveness of the reconstruction algorithm, i.e., Algorithm 1, for which the simulation results are shown in Figure 10. The figure shows that if the noise is small, the recovered signals are extremely close to the original signals, which also verifies the effectiveness of the Cadzow denoising technique for dynamical sampling.

5.3. Real data. In this section, we describe numerical tests that we performed using two sets of real data. One data set documents a cooling process with a single heat source, and the other – a similar process with two heat sources. These data sets were labeled as “one hotspot” and “two hotspots”, respectively.

The set-up for the real data sets is shown in Figure 11. We used the bicycle (aluminum) wheel for the circular pattern. Fifteen (15) sensors are equidistantly

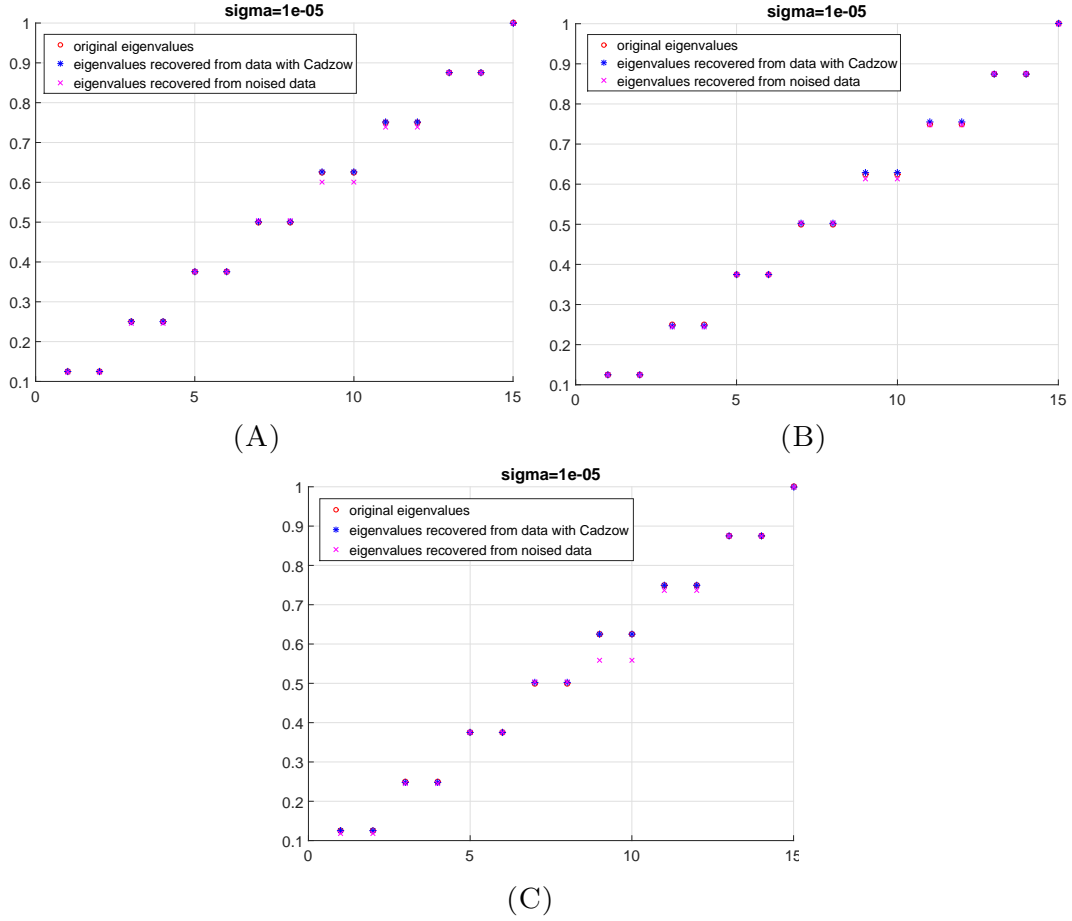


FIGURE 7. A comparison of the spectrum reconstruction with and without the Cadzow denoising technique for $\sigma = 10^{-5}$.

placed around the perimeter of the wheel with 4.5 inches apart. The specified accuracy of the sensors is $0.5^{\circ}C$ and the temperature samples are taken at 1.05Hz.

The goal was to estimate the dynamical operator and the original signals by using information from a subset of the thermometer measuring devices, while the totality of the measurements from all devices was used as control to assess the performance of our estimations. In our reconstructions, we did not use any a priori knowledge about the conducting material, its parameters, or the underlying operator driving the evolution of the temperature. Only raw, time-space subsamples of the temperatures was used to estimate the evolution operator, and the initial temperature distribution. The operator was assumed to be real, symmetric convolution operator whose Fourier transform consists of two monotonic pieces, so that recovery of the spectrum of the driving operator sufficed to recover the filter.

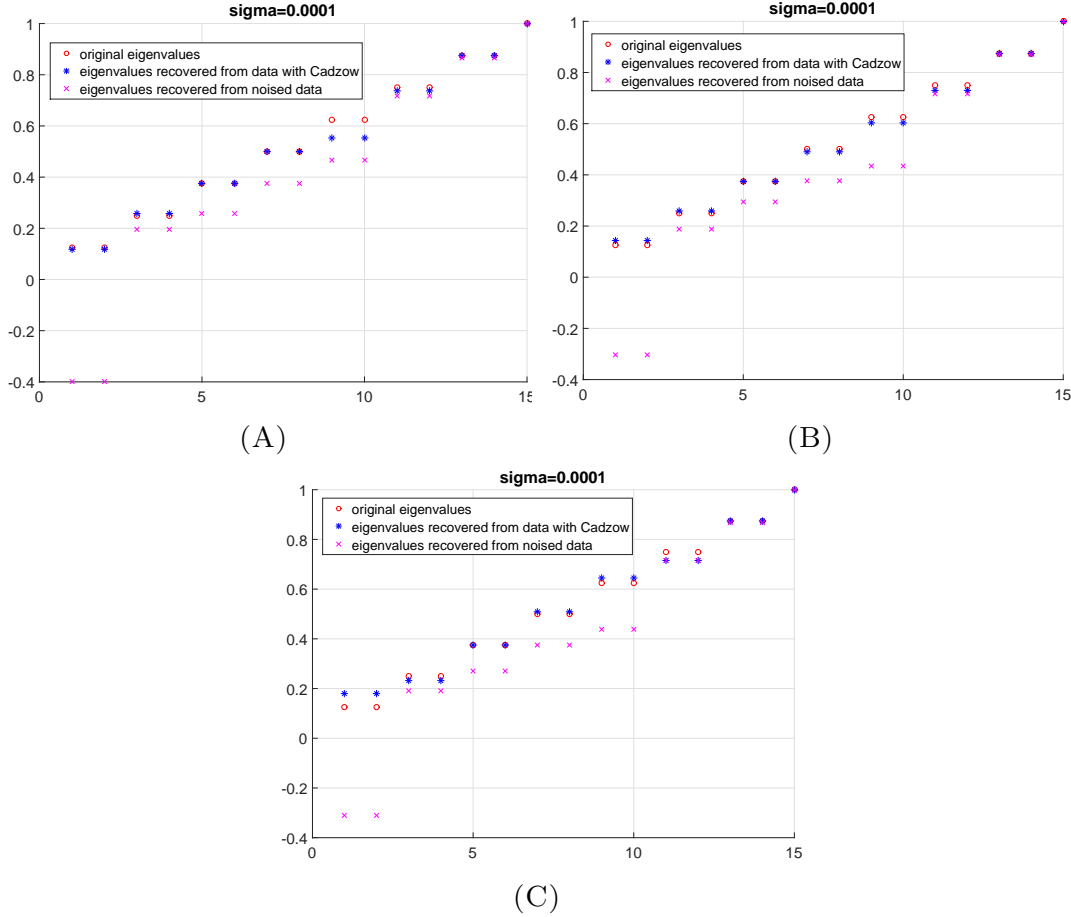


FIGURE 8. A comparison of the spectrum reconstruction with and without the Cadzow denoising technique for $\sigma = 10^{-4}$.

In the experiment, the signal at time level 20 was set as the original state. First, we smoothed the data by averaging over time to obtain a new data set $\Gamma = (\gamma_1 \ \gamma_2 \ \dots)$, where $\gamma_1 = \sum_{i=1}^{10} f_i$, $\gamma_2 = \sum_{i=11}^{20} f_i$, etc. Next, we extracted the information from the new data set at uniform locations Ω with gap $m = 3$ generating the data set $S_m(\Gamma)$. Cadzow Algorithm 3 is then used on $\tilde{Y} = S_m(\Gamma)$ with the threshold rank close to 2 or 3 to obtain the denoised data Z . Using the data Z , Algorithm 2 was applied to estimate the filter. Finally, using the recovered filter, the original signals were estimated by repeating the computations as in Section 5.1.

The test results on the data set with one hotspot are shown in Figure 12. Figure 12A depicts the evolved signals at all 15 locations. Figure 12B shows the recovered spectrum of the evolution filter using the data from locations $\Omega = \{1, 4, 7, 10, 13\}$ to estimate the filter driving the system. Using the driving operator A recovered from Ω and the necessary extra sampling locations at $\{3, 15\}$ needed to recover

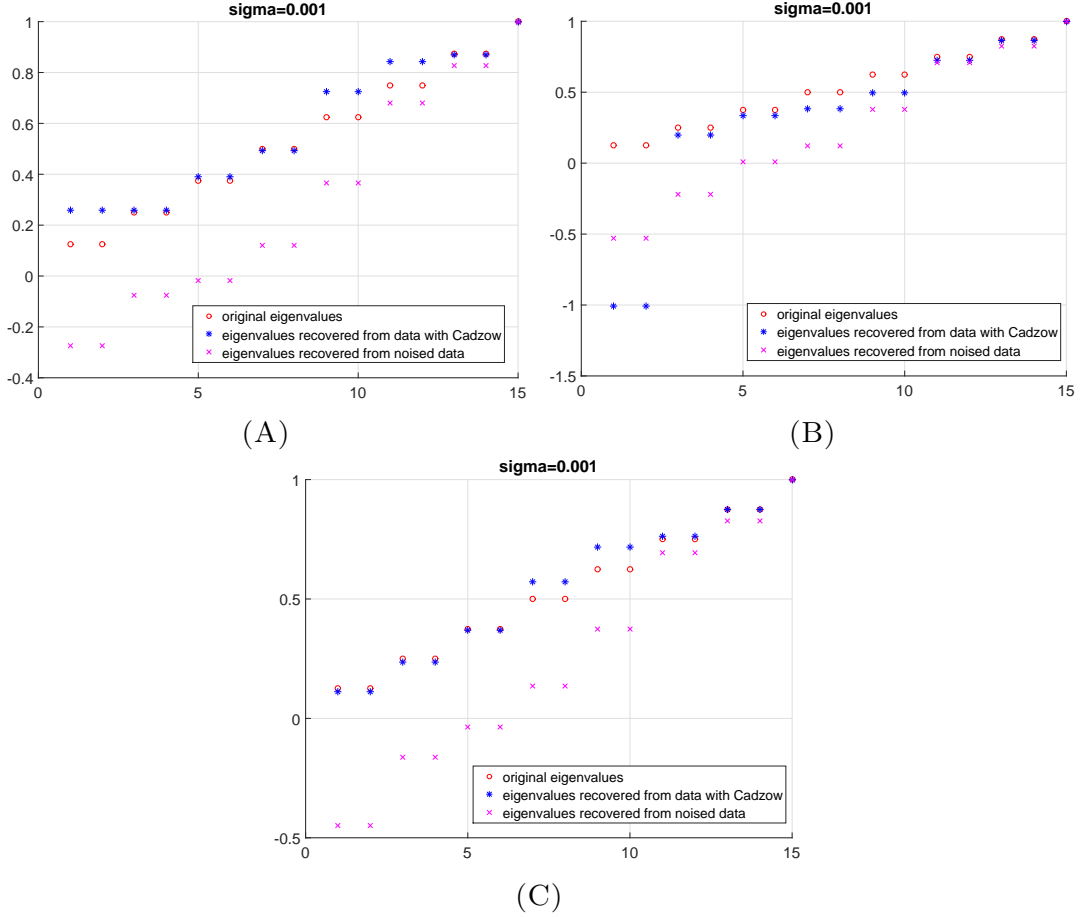


FIGURE 9. A comparison of the spectrum reconstruction with and without the Cadzow denoising technique for $\sigma = 10^{-3}$.

the signal ($\Omega_e = \Omega \cup \{3, 15\}$) (see [5]), we reconstructed an approximation $f^\#$ of the signal that is displayed in Figure 12C; it has a relative error $\frac{\|\gamma_1 - f^\#\|_2}{\|\gamma_1\|_2}$ of 9.94% compared to the actual measurements at all 15 locations as the reference. This relative error shows that dynamical sampling also works reasonably well for a real data set.

The test results using the data set with two hotspots are shown in Figure 13. Figure 13A plots the evolved signals at the 15 locations. Figure 13B exhibits the recovered spectrum of the filter with $\Omega = \{2, 5, 8, 11, 14\}$. Using the driving operator A recovered from Ω and the data from locations $\Omega_e = \{2, 3, 5, 8, 10, 11, 14\}$, we recovered an approximation of the signal that is displayed in Figure 13C. In this case, the relative error was 12.45% compared to the actual measurements at all 15 locations. Such relative error is generally considered acceptable in this kind of real applications.

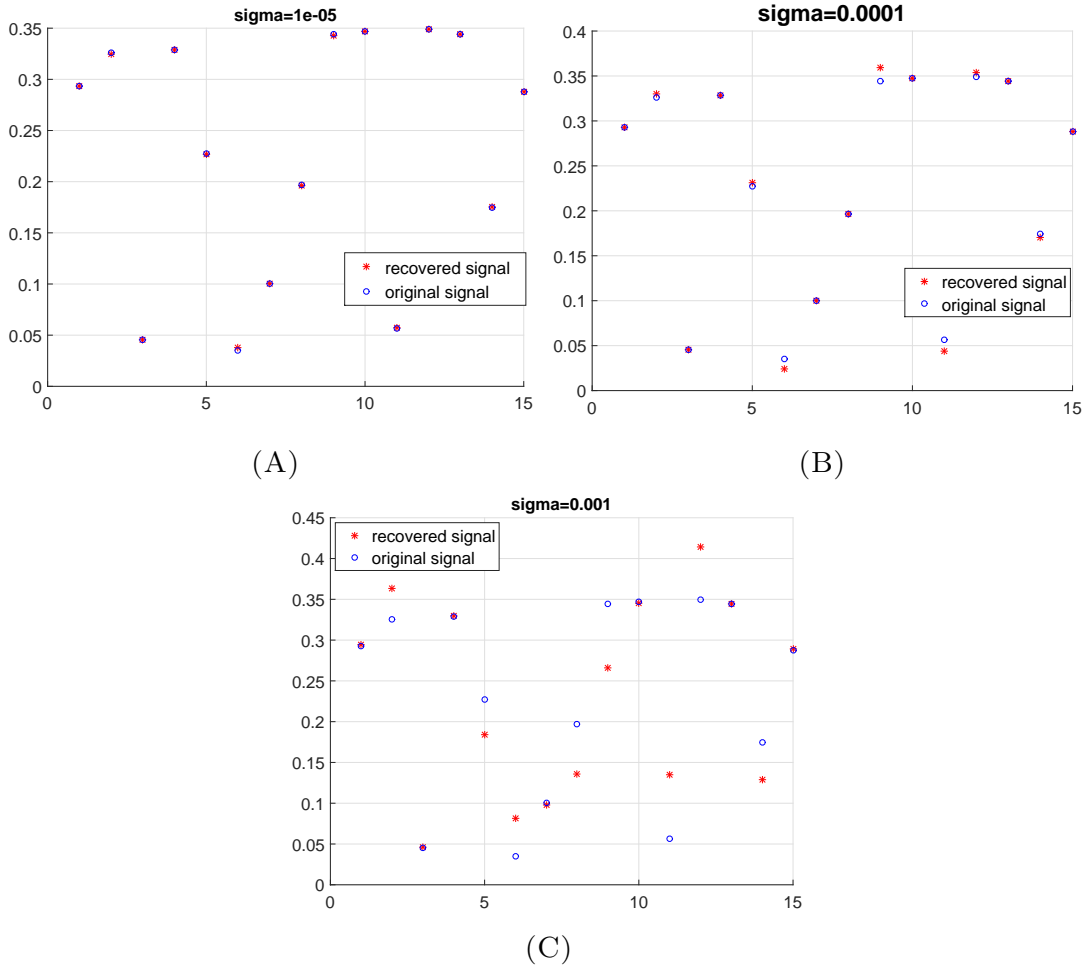
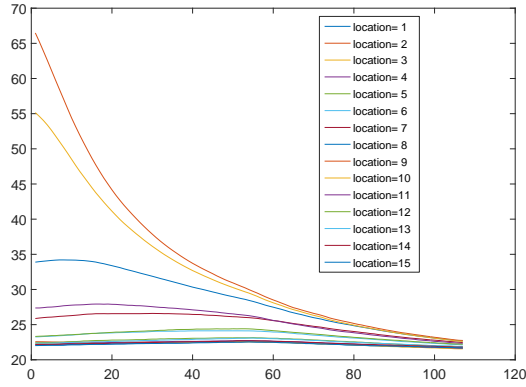


FIGURE 10. A comparison of the recovered signal and the original signal by using the estimated recovered convolution operator.

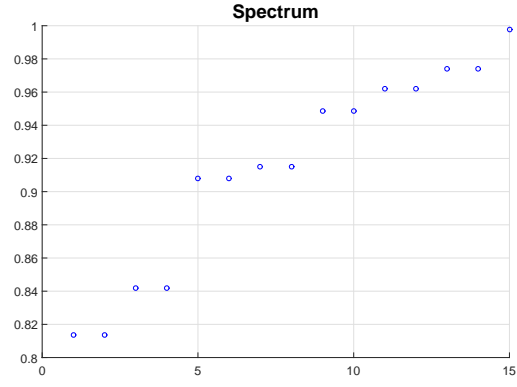
By making similar tests with different choices of Ω and Ω_e , we found that the relative errors depend heavily on the choice of locations. The two pictures in Figure 14 are the results of the same process that was used to generate the last two pictures in Figure 12. In this case, however, we chose $\Omega = \{2, 5, 8, 11, 14\}$ and $\Omega_e = \{2, 3, 5, 8, 10, 11, 14\}$. This choice resulted in the relative error of 34.29% which is considerably larger than the 9.94% in Figure 12.



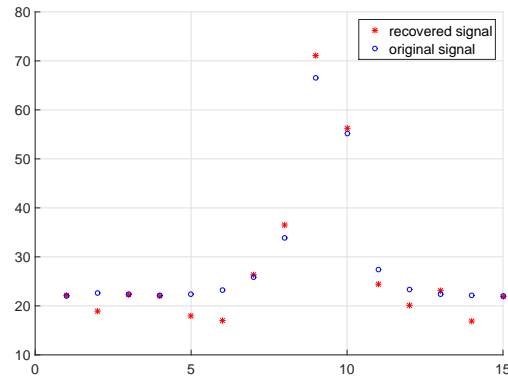
FIGURE 11. Set-up.



(A)



(B)



(C)

FIGURE 12. Simulation results for the data set with one hotspot. Here, (12A) plots the evolved signals, (12B) shows the recovered spectrum by using the data from partial locations, and (12C) sketches the recovered signal by using the recovered operator from partial locations and the sampled original signal. The partial locations for recovering the operator are $\Omega = \{1, 4, 7, 10, 13\}$. To recover the original signals, we use the data from locations $\Omega_e = \{1, 3, 4, 7, 10, 13, 15\}$.

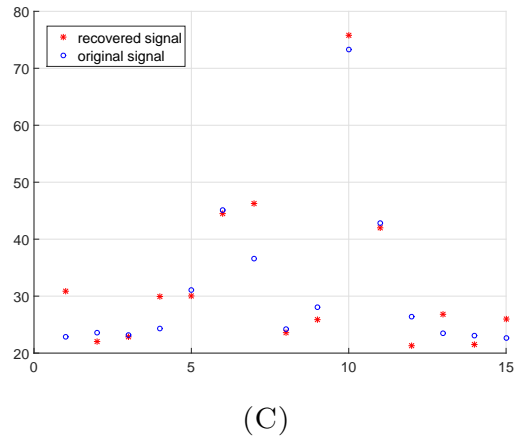
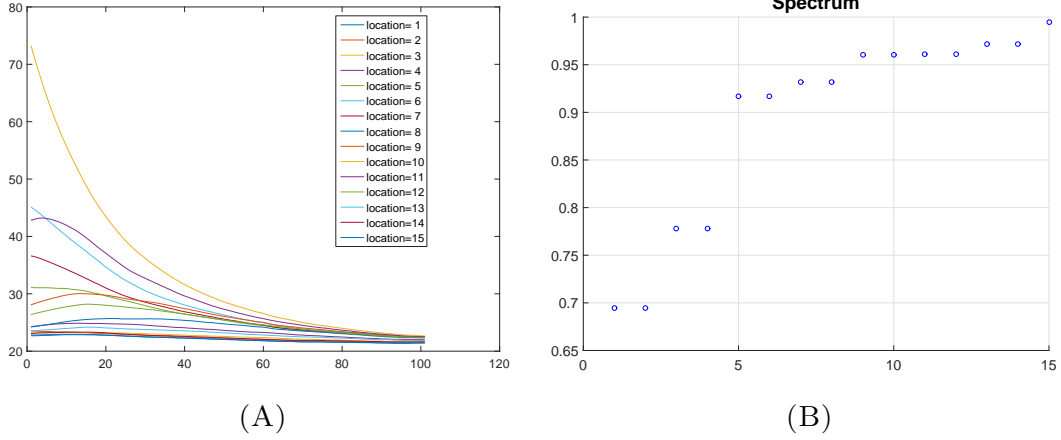


FIGURE 13. Simulation results for the data set with two hotspots. Here, (13A) plots the evolved signals, (13B) shows the recovered spectrum by using the data from partial locations, and (13C) sketches the recovered signal by using the recovered operator from partial locations and the sampled original signal. The partial locations for recovering the operator are $\Omega = \{2, 5, 8, 11, 14\}$. To recover the original signals, we use the data from locations $\Omega_e = \{2, 3, 5, 8, 10, 11, 14\}$.

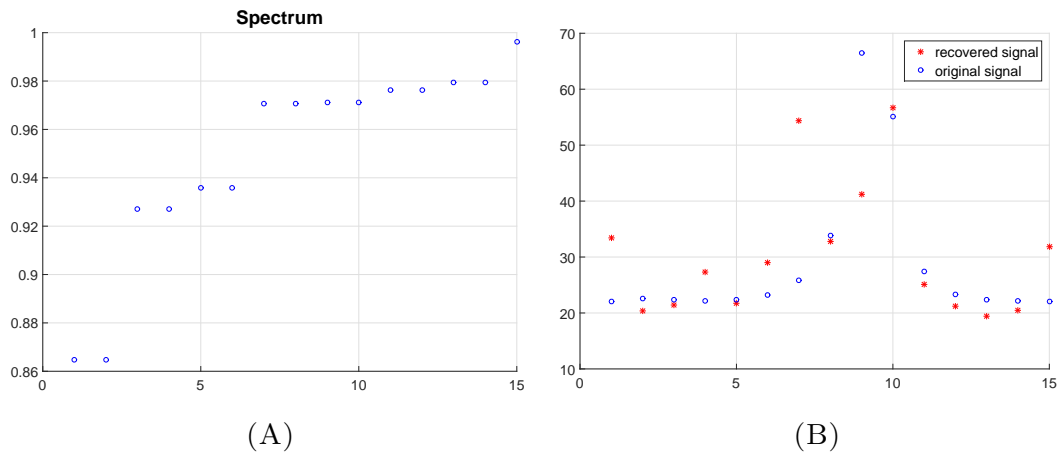


FIGURE 14. Simulation results for the data set with one hotspot. Here, (14A) shows the recovered spectrum by using the data from partial locations, while (14B) plots the recovered signal by using the recovered operator from partial locations, where the partial locations for recovering the operator are $\Omega = \{2, 5, 8, 11, 14\}$. To recover the original signals, we use the samples from locations $\Omega_e = \{2, 3, 5, 8, 10, 11, 14\}$.

6. CONCLUDING REMARKS

This paper introduces the problem of noise into the modeling of dynamical sampling and discusses certain unbiased linear estimators for the recovery of signals from dynamical sampling. The addition of noise to the model highlights some of the difficulties in recovering a signal from measurements in dynamical sampling, and sets the stage for more detailed studies of the information theoretic bounds and other types of estimators.

In addition, this paper studies a special case related to blind deconvolution, where the subsampling is uniform (to which extra samples are added for the recovery of the unknown signal), and the evolution operator is unknown, but is one dimensional, symmetric, real and decreasing in the frequency domain. The existence of multiple measurements over time, along with the assumptions on the properties of the filter, allow for the recovery of the unknown signal and unknown filter; we point to some of the factors that have an adverse effect on the stability of this procedure.

The basic algorithms and discussion of certain special cases are presented here with the intent of providing a starting point for future work on both the theoretical and algorithmic aspects of noisy instances of dynamical sampling and the case where the evolution operator is unknown.

Acknowledgement

The research is supported by the collaborative NSF ATD grant DMS-1322099 and DMS-1322127. We would like to thank the organizers of SampTA 2017 in Estonia and CIMPA 2017 in Argentina for their hospitality. We would also like to thank Miklos Maroti and the anonymous reviewers for helpful comments and suggestions. Special thanks are reserved to S. J. Rose for imparting his wisdom, as generously as ever.

APPENDIX A. PROOF OF PROPOSITION 4.1

Proof of Proposition 4.1. It is clear that

$$\begin{aligned} \|\epsilon_L\|_2^2 &= \left\| \left(\sum_{i=1}^L A_i^* A_i \right)^{-1} \left(\sum_{j=1}^L A_j^* \eta_j \right) \right\|_2^2 \\ &= \sum_{j=1}^L \left\| \left(\sum_{i=1}^L A_i^* A_i \right)^{-1} A_j^* \eta_j \right\|_2^2 + \sum_{j \neq k} \left\langle \left(\sum_{i=1}^L A_i^* A_i \right)^{-1} A_j^* \eta_j, \left(\sum_{i=1}^L A_i^* A_i \right)^{-1} A_k^* \eta_k \right\rangle. \end{aligned}$$

Since η_j and η_k for $j \neq k$ are independent and mean zero, the cross terms cancel out in expectation, and one has

$$E \left(\left\langle \left(\sum_{i=1}^L A_i^* A_i \right)^{-1} A_j^* \eta_j, \left(\sum_{i=1}^L A_i^* A_i \right)^{-1} A_k^* \eta_k \right\rangle \right) = 0.$$

Consequently,

$$(A.1) \quad E(\|\epsilon_L\|_2^2) = \sum_{j=1}^L E \left(\left\| \left(\sum_{i=1}^L A_i^* A_i \right)^{-1} A_j^* \eta_j \right\|_2^2 \right).$$

Note that

$$\begin{aligned} & \left\| \left(\sum_{i=1}^L A_i^* A_i \right)^{-1} A_j^* \eta_j \right\|_2^2 = \left\| \left(\sum_{i=1}^L A_i^* A_i \right)^{-1} \sum_{l=1}^{m_j} A_j^{*(l)} \eta_j^l \right\|_2^2 \\ &= \sum_{l=1}^{m_j} \left\| \left(\sum_{i=1}^L A_i^* A_i \right)^{-1} A_j^{*(l)} \eta_j^l \right\|_2^2 + \sum_{l \neq p} \left\langle \left(\sum_{i=1}^L A_i^* A_i \right)^{-1} A_j^{*(l)} \eta_j^l, \left(\sum_{i=1}^L A_i^* A_i \right)^{-1} A_j^{*(p)} \eta_j^p \right\rangle, \end{aligned}$$

where $A_j^{*(l)}$ denotes the l -th column of matrix A_j^* and η_j^l is the l -th entry of η_j . Additionally, η_j^l and η_j^p are independent for $l \neq p$. It follows that

$$E \left(\left\langle \left(\sum_{i=1}^L A_i^* A_i \right)^{-1} A_j^{*(l)} \eta_j^l, \left(\sum_{i=1}^L A_i^* A_i \right)^{-1} A_j^{*(p)} \eta_j^p \right\rangle \right) = 0.$$

Thus,

$$\begin{aligned} E(\|\epsilon_L\|_2^2) &= \sum_{j=1}^L \sum_{l=1}^{m_j} E \left(\left\| \left(\sum_{i=1}^L A_i^* A_i \right)^{-1} A_j^{*(l)} \eta_j^l \right\|_2^2 \right) \\ &= \sigma^2 \sum_{j=1}^L \sum_{l=1}^{m_j} \left\| \left(\sum_{i=1}^L A_i^* A_i \right)^{-1} A_j^{*(l)} \right\|_2^2 \\ &= \sigma^2 \cdot \sum_{j=1}^L \text{trace} \left(A_j \left(\sum_{i=1}^L A_i^* A_i \right)^{-2} A_j^* \right) \\ &= \sigma^2 \cdot \text{trace} \left(\left(\sum_{j=1}^L A_j^* A_j \right) \left(\sum_{i=1}^L A_i^* A_i \right)^{-2} \right) \end{aligned}$$

$$(A.2) \quad = \sigma^2 \cdot \text{trace} \left(\left(\sum_{i=1}^L A_i^* A_i \right)^{-1} \right) = \sigma^2 \sum_{i=1}^d 1/\lambda_i(L)$$

and the proposition is proved. \square

REFERENCES

- [1] R. ACESKA, A. PETROSYAN, AND S. TANG, *Multidimensional signal recovery in discrete evolution systems via spatiotemporal trade off*, *Sampl. Theory Signal Image Process.*, 14 (2015), pp. 153–169.
- [2] R. ACESKA AND S. TANG, *Dynamical sampling in hybrid shift invariant spaces*, vol. 626 of *Contemp. Math.*, Amer. Math. Soc., Providence, RI, 2014.
- [3] A. ALDROUBI, C. CABRELLI, A. ÇAKMAK, U. MOLTER, AND A. PETROSYAN, *Iterative actions of normal operators*, *J. Funct. Anal.*, 272 (2017), pp. 1121–1146.
- [4] A. ALDROUBI, C. CABRELLI, U. MOLTER, AND S. TANG, *Dynamical sampling*, *Applied and Computational Harmonic Analysis*, 42 (2017), pp. 378–401. doi: 10.1016/j.acha.2015.08.014.
- [5] A. ALDROUBI, J. DAVIS, AND I. KRISHTAL, *Dynamical sampling: time-space trade-off*, *Appl. Comput. Harmon. Anal.*, 34 (2013), pp. 495–503.
- [6] A. ALDROUBI, J. DAVIS, AND I. KRISHTAL, *Exact reconstruction of signals in evolutionary systems via spatiotemporal trade-off*, *Journal of Fourier Analysis and Applications*, 21 (2015), pp. 11–31.
- [7] A. ALDROUBI, L. HUANG, I. KRISHTAL, AND R. LEDERMAN, *Dynamical sampling with random noise*, in *2017 International Conference on Sampling Theory and Applications (SampTA)*, July 2017, pp. 409–412.
- [8] A. ALDROUBI AND I. KRISHTAL, *Krylov subspace methods in dynamical sampling*, *Sampl. Theory Signal Image Process.*, 15 (2016), pp. 9–20.
- [9] A. ALDROUBI, I. KRISHTAL, AND S. TANG, *Phase retrieval of evolving signals from space-time samples*, in *2017 International Conference on Sampling Theory and Applications (SampTA)*, July 2017, pp. 46–49.
- [10] A. ALDROUBI, I. KRISHTAL, AND E. WEBER, *Finite dimensional dynamical sampling: an overview*, in *Excursions in harmonic analysis. Volume 4*, *Appl. Numer. Harmon. Anal.*, Birkhäuser/Springer, New York, 2015, ch. XV, pp. 231–244. DOI: 10.1007/978-3-319-20188-7.9.
- [11] A. BJÖRCK, *A general updating algorithm for constrained linear least squares problems*, *SIAM J. Sci. Statist. Comput.*, 5 (1984), pp. 394–402.
- [12] J. CADZOW, *High performance spectral estimation—a new ARMA method*, *IEEE Trans. Acoust. Speech Signal Process.*, 28 (1980), pp. 524–529.
- [13] C. CABRELLI, U. MOLTER, V. PATERNOSTRO, AND F. PHILIPP, *Dynamical Sampling on Finite Index Sets*, *ArXiv e-prints*, (2017).
- [14] O. CHRISTENSEN AND M. HASANNASAB, *Operator Representations of Frames: Boundedness, Duality, and Stability*, *Integral Equations Operator Theory*, 88 (2017), pp. 483–499.
- [15] J. DAVIS, *Dynamical sampling with a forcing term*, vol. 626 of *Contemp. Math.*, Amer. Math. Soc., Providence, RI, 2014.
- [16] J. GILLARD, *Cadzow’s basic algorithm, alternating projections and singular spectrum analysis*, *Stat. Interface*, 3 (2010), pp. 335–343.
- [17] G. H. GOLUB AND C. F. V. LOAN, *Matrix computations*, *Johns Hopkins Studies in the Mathematical Sciences*, Johns Hopkins University Press, Baltimore, MD, fourth ed., 2013.

- [18] K. GRÖCHENIG, J. ROMERO, J. UNNIKRISSHANN, AND M. VETTERLI, *On minimal trajectories for mobile sampling of bandlimited fields*, Appl. Comput. Harmon. Anal., 39 (2015), pp. 487–510.
- [19] D. KUNDUR AND D. HATZINAKOS, *Blind image deconvolution*, IEEE signal processing magazine, 13 (1996), pp. 43–64.
- [20] J. MURRAY-BRUCE AND P. DRAGOTTI, *Estimating localized sources of diffusion fields using spatiotemporal sensor measurements*, IEEE Trans. Signal Process., 63 (2015), pp. 3018–3031.
- [21] ———, *A sampling framework for solving physics-driven inverse source problems*, IEEE Transactions on Signal Processing, 65 (2017), pp. 6365–6380.
- [22] F. PHILIPP, *Bessel orbits of normal operators*, J. Math. Anal. Appl., 448 (2017), pp. 767–785.
- [23] ———, *Bessel orbits of normal operators*, Journal of Mathematical Analysis and Applications, 448 (2017), pp. 767 – 785.
- [24] J. RICE, *Mathematical Statistics and Data Analysis*, Duxbury Advanced Series, 3 ed., 2007. ISBN 0-534-39942-8.
- [25] S. TANG, *System identification in dynamical sampling*, Adv. Comput. Math., (to appear). ArXiv:1502.02741.
- [26] Q. ZHANG, R. LI, AND B. LIU, *Periodic nonuniform dynamical sampling in $\ell^2(\mathbb{Z})$ and shift-invariant spaces*, Numerical Functional Analysis and Optimization, 38 (2017), pp. 395–407.
- [27] Q. ZHANG, B. LIU, AND R. LI, *Dynamical sampling in multiply generated shift-invariant spaces*, Applicable Analysis, 96 (2017), pp. 760–770.